Downloaded from UvA-DARE, the institutional repository of the University of Amsterdam (UvA)
http://hdl.handle.net/11245/2.12733

File ID	uvapub:12733
Filename	88343y.pdf
Version	unknown

SOURCE (OR PART OF THE FOLLOWING SOURCE):

Type	article
Title	Orbital dynamics of Cygnus X-3
Author(s)	M.M. Hanson, M.D. Still, R.P. Fender
Faculty	FNWI: Astronomical Institute Anton Pannekoek (IAP)
Year	2000

FULL BIBLIOGRAPHIC DETAILS:
http://hdl.handle.net/11245/1.175633

Copyright

It is not permitted to download or to forward/distribute the text or part of it without the consent of the author(s) and/or copyright holder(s), other than for strictly personal, individual use, unless the work is under an open content licence (like Creative Commons).

UvA-DARE is a service provided by the library of the University of Amsterdam (http://dare.uva.nl)
(pagedate: 2014-11-15)

THE ASTROPHYSICAL JOURNAL, 541:308–318, 2000 September 20
© 2000. The American Astronomical Society. All rights reserved. Printed in U.S.A.

ORBITAL DYNAMICS OF CYGNUS X-3

M. M. HANSON,[1] M. D. STILL,[2,3] AND R. P. FENDER[4]
Received 2000 February 7; accepted 2000 April 21

ABSTRACT

Orbital-phase–resolved infrared spectra of Cygnus X-3 in outburst and quiescence, including tomographic analysis, are presented. We confirm the phasing of broad He II and N V lines in quiescence, such that maximum blueshift corresponds to the X-ray minimum at $\Phi = 0.00 \pm 0.04$. In outburst, double-peaked He I structures show a similar phasing with two significant differences: (1) although varying in relative strength, there is continuous line emission in blue and red peaks around the orbit; and (2) an absorption component, $\sim\frac{1}{4}$ of an orbit out of phase with the emission features, is discerned. Doppler tomograms of the double-peaked profiles are consistent with a disk-wind geometry, rotating at velocities of 1000 km s^{-1}. Regrettably, the tomography algorithm will produce a similar ring structure from alternative line sources if contaminated by overlying P Cygni profiles. This is certainly the case in the strong 2.0587 μm He I line, leading to an ambiguous solution for the nature of double-peaked emission. The absorption feature, detected $\frac{1}{4}$ of an orbit out of phase with the emission features, is consistent with an origin in the He star wind and yields for the first time a plausible radial velocity curve for the system. We directly derive the mass function of the system, 0.027 $M_\odot$. If we assume a neutron star accretor and adopt a high orbital inclination, $i > 60°$, we obtain a mass range for the He star of $5\ M_\odot \lesssim M_{\rm WR} \lesssim 11\ M_\odot$. Alternatively, if the compact object is a black hole, we estimate $M_{\rm BH} \lesssim 10\ M_\odot$. We discuss the implications of these masses for the nature and size of the binary system.

Subject headings: binaries: close — circumstellar matter — infrared: stars — stars: individual (Cygnus X-3)

On-line material: color figures

1. INTRODUCTION

First discovered in the pioneering X-ray surveys of the 1960s, Cygnus X-3 (Cyg X-3) remains among the least understood of the long-standing X-ray sources known in the sky. In the early 1970s, it was discovered to show a flux modulation on a period of 4.8 hr, first in X-rays (Parsignault et al. 1972; Sanford & Hawkins 1972) and then also at near-infrared wavelengths (Becklin et al. 1973), which was assumed to be the orbital period of the binary system. Modulation of the light curve at this period is asymmetric and extremely similar in both X-ray and infrared bands (Mason, Cordova, & White 1986), with the exception of irregular, rapid flaring superposed on the orbital modulation in the infrared (Mason et al. 1986; Fender et al. 1996). The period of this orbit was further shown to be rapidly increasing, with a timescale of just 850,000 yr (Kitamoto et al. 1995).

Van den Heuvel & De Loore (1973) made the prediction that the system was composed of a compact object and a helium star, thus representing a remarkably rare, late evolutionary stage of a massive X-ray binary. Nearly 20 years later, persuasive evidence to support this prediction was found in near-infrared spectroscopic data presented by van Kerkwijk et al. (1992, 1996). They discovered strong, broad emission lines of neutral and ionized helium, combined with a marked lack of hydrogen features. These properties are reminiscent of massive, highly evolved stars known as Wolf-Rayet stars (Smith 1968). As such, Cyg X-3 represents one of the most unique binary systems in our Galaxy. Should the helium companion star become a supernova, as is generally predicted for Wolf-Rayet stars (however, cf. Conti 1996), it could evolve into a double compact object binary system, such as the Hulse-Taylor pulsar, PSR 1913+16 (Hulse & Taylor 1975; Burrows & Woosley 1986). In addition, Cyg X-3 is one of the most luminous sources of radio jets in our Galaxy, displaying repeated ejections at (probably) relativistic velocities (e.g., Schalinski et al. 1998).

While much data have been gathered on the system through X-ray, near-infrared, and radio observations, the most fundamental properties of the Cyg X-3 system have been difficult to constrain. This is a consequence of line emission found to be dominated by a nonaxisymmetric wind component rather than one or both of the stellar objects. Furthermore, the wind features are generally weak, very broad, and at times heavily blended, making line identification difficult or impossible. Consequently, stellar masses have not been measured from binary motion. There exist plausible arguments for both a high- (Schmutz, Geballe, & Schild 1996) and low- (Mitra 1996, 1998) mass companion star, which has inevitable consequences for the state of the compact object, be it a neutron star or a black hole. As the only known Wolf-Rayet + compact object binary and (probably) the shortest period high-mass X-ray binary, accurate constraints on the mass and dimensions of the Cyg X-3 system are crucial for our understanding of many aspects of massive binary evolution.

In a previous paper (Fender, Hanson, & Pooley 1999, hereafter FHP99), we found a dramatic spectral change during an outburst of the system. Though the lines suffer from serious blending, it would appear that during outburst the spectrum of the system evolves from showing high-excitation single-peaked emission lines to one dominated by

[1] Department of Physics, University of Cincinnati, Cincinnati, OH 45221-0011.

[2] NASA Goddard Space Flight Center, Code 662, Greenbelt, MD 20771.

[3] Universities Space Research Association.

[4] Astronomical Institute "Anton Pannekoek," University of Amsterdam, and Center for High Energy Astrophysics, Kruislaan 403, 1098 SJ Amsterdam, The Netherlands.

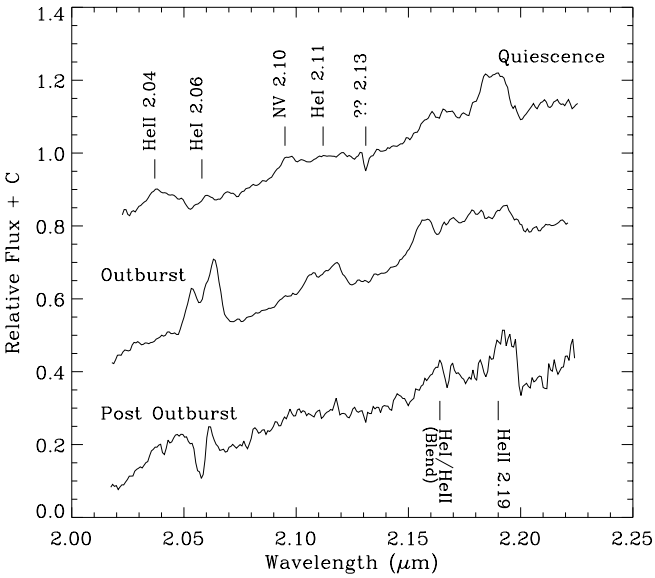

FIG. 1.—*K*-band spectra of Cyg X-3, each displayed with an arbitrary flux offset *C* for clarity. The quiescent spectrum shown at top was taken 1996 June 6 (epoch A, as defined by FHP99). The middle spectrum was taken 1997 June 19 (epoch C) during very extreme radio and X-ray flaring of the system. The bottom spectrum was taken 1997 October 15 (epoch D). During this time, small X-ray flaring was still occurring, but the system was now in "postoutburst."

low-excitation double-peaked profiles. In the current paper we present a first analysis of these data in order to map the velocity field of the line-emitting regions.

2. OBSERVATIONS

We have recently completed a monitoring program of the Cyg X-3 system spanning 18 months. Our observations are based on broadband radio observations at 15 GHz combined with the *Rossi X-Ray Timing Explorer* All-Sky Monitor program (FHP99). During this monitoring program we obtained the best near-infrared spectroscopy of the system, intermittently throughout the 18 months. These data, comprising over 100 individual spectra taken of Cyg X-3, were obtained over four different observing campaigns between 1996 May and 1997 October. The data are available through the CDS archive Web site (see FHP99).

The near-infrared spectroscopic data used in this analysis are presented and fully described in FHP99. Observations were made using the Steward Observatory's infrared spectrometer, FSpec (Williams et al. 1993), on the Multiple Mirror Telescope, prior to the recent upgrade to a single mirror. The spectra have an effective resolution of $R \approx 1200$ at 2.12 μm and a spectral coverage from 2.02 to 2.22 μm. Our analysis in this paper is based on epochs A, C, and D, as defined by FHP99. The Cyg X-3 system was in quiescent, outburst, and postoutburst mode, respectively, during these three epochs. Figure 1 displays spectra taken from each epoch in order to show the main spectral features present during these three epochs. In quiescence the *K* band is dominated by broad, weak He II and N V emission; in outburst strong, twin-peaked He I emission dominates. For a detailed discussion see FHP99.

3. ANALYSIS

Because of the night-to-night variations of the emission-line profiles observed during the outburst phase (see FHP99), it was important to obtain full orbital coverage on a single night for this analysis. We have time-resolved spectra providing full orbital sampling during two nights, 1996 June 2–3, when the system was in quiescence, and 1997 June 19–20, when the system was in outburst. Despite the heavy blending, we were able to identify a few of the major features within the spectra using the laboratory transition lists of Morris et al. (1996).

3.1. *1996 June Quiescent Spectra*

Trailed spectra from 1996 June are presented in the upper three panels of Figure 2. In each case, the continuum was removed by subtracting a three-spline fit to nearby line-free wavelength regions, and the data were recast into constant velocity bins of 121 km s^{-1}. Spectra were further mean averaged into 10 orbital phase bins using the ephemeris of Kitamoto et al. (1995). Doppler tomograms were constructed from the trailed spectra using the maximum entropy method (Marsh & Horne 1988), an approach preferred here over other mapping algorithms because it allows the mapping of blended lines such as the He II 2.1653, 2.1891 μm doublet. It involves the transformation of velocity phase information provided by the Doppler-broadened emission-line profiles (V, Φ) to a velocity-velocity field (V_x, V_y) using

$$f(V, \Phi) = \iint I(V_x, V_y) \times g(V - \gamma + V_x \cos \Phi - V_y \sin \Phi) dV_x dV_y . \quad (1)$$

The mapping results from a χ^2 iteration between model and a fit and entropy minimization (Skilling & Bryan 1984). The term f is the emission-line intensity at velocity V and orbital phase Φ, I the emission distribution of the resulting map in velocity coordinates (V_x, V_y), γ the systemic velocity of the binary center of mass, and $g(V)$ the local line profile. From the combination of Doppler-broadened line profiles and rotational profile variations over the orbit, the maps are reconstructions of line emission in the velocity field around the binary, where V_y is the velocity in the direction parallel to a line joining the two stellar centers and V_x is the velocity orthogonal to V_y in the plane of the orbit.

Any motion out of the orbital plane will not be recognized by the mapping, and consequently Doppler tomograms are of most use in systems where line emission is confined to gas moving in a plane, such as when it is distributed over an accretion disk or one of the stellar companions. If emission originates in a spherical wind, the tomograms become difficult, if not impossible, to interpret with any confidence. Our motivation for applying tomographic mapping to the lines in Cyg X-3 is twofold. First, in quiescence the line-emitting wind region is thought to be within the cone shadowed from the X-ray source by the companion star (van Kerkwijk et al. 1996). Motion in the cone is somewhat constrained to the orbital plane, although this assumption breaks down if the mass ratio $q = M_{\rm WR}/M_{\rm X}$ is too large. Second, FHP99 reveal that line emission profiles are double-peaked in outburst, suggesting that a disk or flattened, rotating wind may dominate profiles during these epochs, in which case Doppler tomography is well suited to these spectra.

The tomograms derived from the quiescent data of Figure 2 are shown in Figure 3. The reduced χ^2 values of

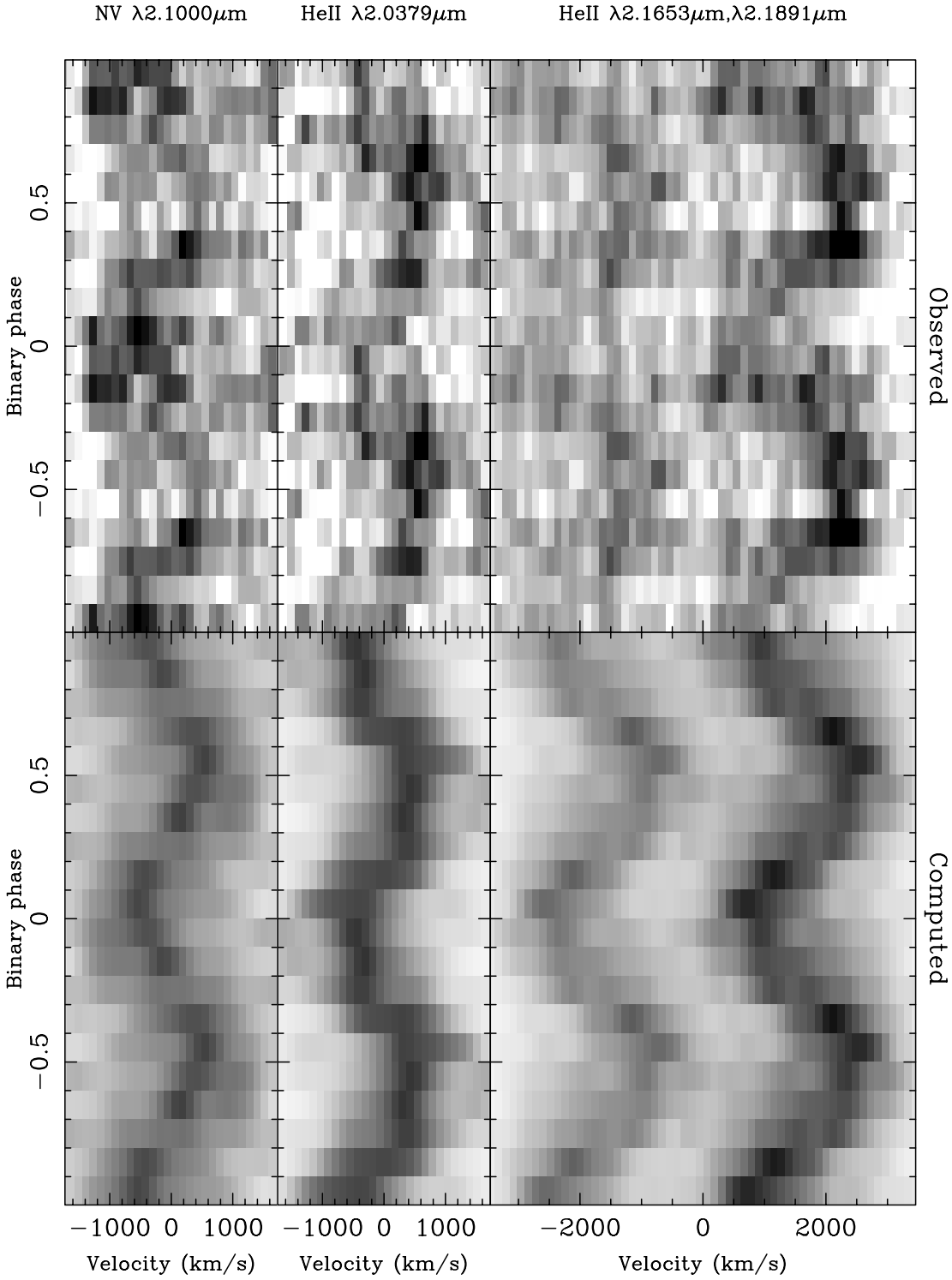

FIG. 2.—*K*-band trailed spectrograms representing full orbital phase coverage (4.8 hr) obtained on 1996 June 2. Spectral regions sampling the four strongest emission features of N v and He II are displayed. The data have been repeated over a second orbital cycle. These data were obtained while Cyg X-3 was in quiescence, as deemed by low radio and X-ray activity (see FHP99). The lower panel shows the model emission profiles produced from the tomographic fit in Fig. 3. White to black corresponds to increasing emission intensity on individual linear scales. White coincides with the continuum level.

these fits are listed in Table 1. For reference, the binary center of mass occurs at $(V_x, V_y) = (0, 0)$ km s^{-1}. The companion star center of mass corresponds to $(V_x, V_y) = (0, K_{\rm WR})$, where $K_{\rm WR} \geq 0$ is the radial velocity of the Wolf-Rayet star. The compact object center of mass occurs at $(V_x, V_y) = (0, K_{\rm X})$, where $K_{\rm X} \leq 0$ is the radial velocity of the accreting star. The ratio $K_{\rm X}/K_{\rm WR} = q$, where q is the ratio of the stellar masses. Rotating structure around the compact object or W-R star will manifest itself as an annulus on the map, centered on $K_{\rm X}$ or $K_{\rm WR}$. The lower panel of Figure 2 shows the model emission profiles produced from the tomographic fit in Figure 3.

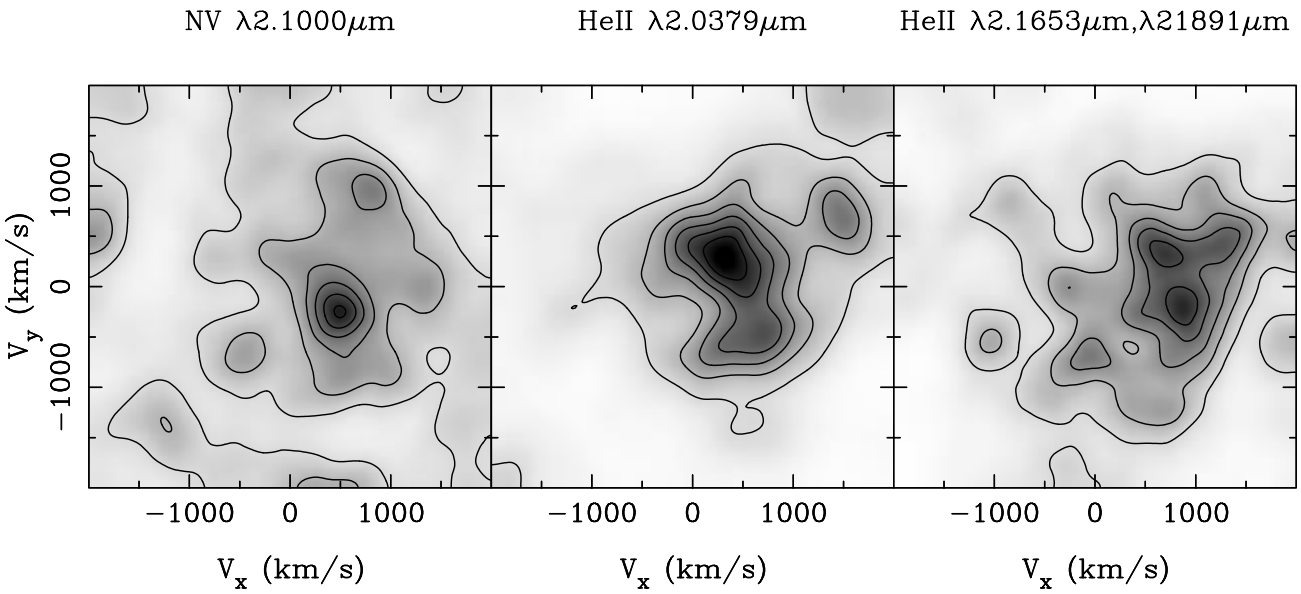

FIG. 3.—Doppler tomograms of the N v and He II lines during quiescence in 1996 June. These are derived from computed fits of the data shown in lower panel of Fig. 2. The intensity scales are as in Fig. 2. The resulting fits from the tomographic modeling (described in eq. [1]) are given in Table 2, and their corresponding reduced χ^2 values are given in Table 1.

The trailed spectra and Doppler tomograms indicate that the line emission in quiescence arises in a restricted region of velocity space. This is consistent with the van Kerkwijk model in which the line emission originates in a region of the stellar wind shadowed from ionizing X-rays by the He star. Note that the cool wind component and binary motion vectors are orthogonal: this results in the wind phasing and W-R star phasing being separated 90° and the tomographic location of the emission occurring in a region offset approximately 90° from the tomographic location of the Wolf-Rayet star. Because of the moderate χ^2 values of these fits, the small-scale structure is not significant.

TABLE 1

χ^2_ν FOR TOMOGRAPHIC FITS

QUIESCENCE		OUTBURST	
Line (μm)	χ^2_ν	Line (μm)	χ^2_ν
N v 2.1000	1.9	He I 2.0587	296.0
He II 2.0379	5.1	He I 2.1126	15.0
He II 2.1653/2.1891	5.2	He I 2.1623/2.1847	31.2

Two-dimensional Gaussian fits to the tomograms provide a first-order estimate of both velocity, $K = (V_x^2 + V_y^2)^{1/2}$, and phasing, $\Phi = \tan^{-1}(V_x/V_y)$, of the emitting gas, and these are listed in Table 2. Uncertainties are not propagated through the mapping algorithm, and therefore the errors are taken to be the size of a pixel element on the maps. Similar results are obtained by fitting one-dimensional, time-dependent Gaussian profiles to the raw data, and this provides confidence in our tomographic fits. These further Gaussian fits are also presented in Table 2, and the resulting velocities plotted against orbital phase are presented in Figure 4.

By taking a variance-weighted mean of the one-dimensional fits, the line-forming region(s) have an average wind velocity of $K = 480 \pm 50$ km s^{-1}. This is consistent with the value measured by Schmutz et al. (1996). We do not detect any significant difference in K between the N v and the three He II lines in this measure. From the fits, an average FWHM value was determined for each of the four transitions and is given in Table 2; if the lines are well represented by Gaussian profiles, these values imply a terminal wind velocity of at least 1500 km s^{-1} in the system, similar to that found by van Kerkwijk et al. (1996).

TABLE 2

LINE IDENTIFICATIONS AND MEASUREMENTS, 1996 JUNE QUIESCENT SPECTRA

		GAUSSIAN FIT				TOMOGRAMS	
λ_{vac} (μm)	Line Identification	γ (km s^{-1})	K (km s^{-1})	FWHM (km s^{-1})	Φ	K (km s^{-1})	Φ
2.0379	He II (15–8)	+162 ± 28	437 ± 36	2959 ± 201	−0.02 ± 0.04	439 ± 20	−0.135 ± 0.05
2.100	N v (11–10)	−108 ± 22	443 ± 25	1928 ± 322	+0.02 ± 0.02	550 ± 20	+0.08 ± 0.04
2.1653[a]	He II (14–8)	−79 ± 39	446 ± 26	1618 ± 124	+0.00 ± 0.04	890 ± 20	+0.03 ± 0.02
2.1891[a]	He II (10–7)	+152 ± 20	577 ± 56	2554 ± 54	+0.16 ± 0.02		

[a] The two lines are partially blended and the tomographic result comes up with a single value for that blend.

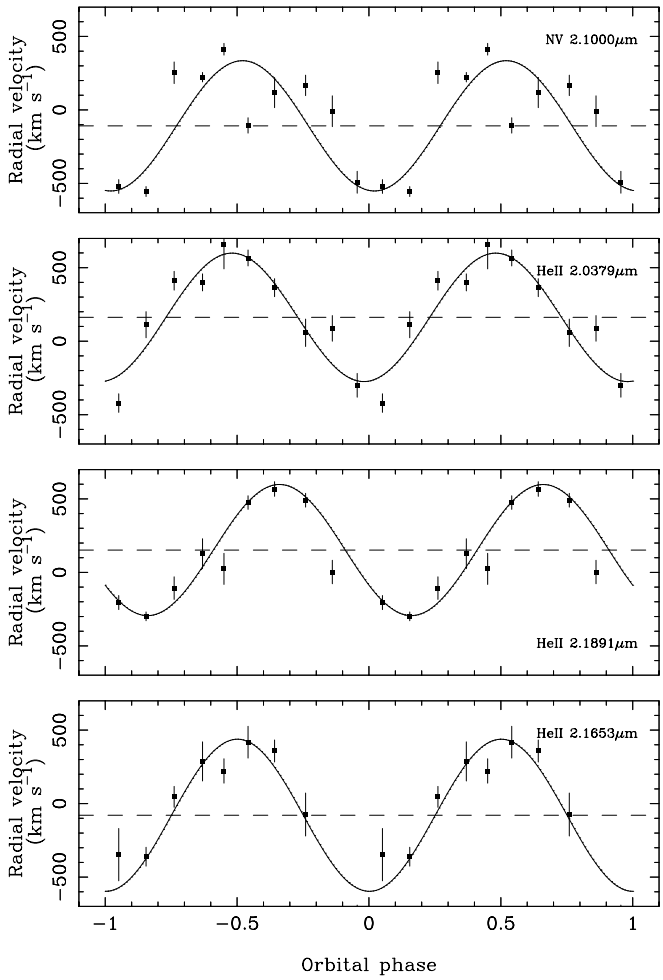

FIG. 4.—Radial velocity fits to the four emission features shown in Fig. 2. Semiamplitude peaks trace general wind velocities, which are also traced in the tomograms of Fig. 3. The velocities determined from this and the tomographic analysis are given in Table 2. *See the electronic edition of the Journal for a color version of this figure.*

We have also more accurately determined the maximum of the blueshifted wind features of He II and N V against the X-ray modulation. From a weighted mean of the four measurements, the He II and N V features are at their maximum blueshift when the X-ray intensity is at a minimum (e.g., $\Phi = 0$), with an error of 0.04 in orbital phase.

Note that there is no well-defined solution for the systemic velocity of the binary center of mass γ (eq. [1]), from the one-dimensional fits in Table 2. This could be the result of turbulence within the wind (e.g., Lépine & Moffat 1999). Furthermore, the laboratory wavelength for the N V transition is not accurately known. The term γ can only be constrained to $|\gamma| \leq 200$ km s^{-1}, precluding us from making a distance estimate. This upper limit on the systemic velocity seems rather difficult to reconcile with the $+800$ km s^{-1} velocity field recently reported by *Chandra* observations of the system (Paerels et al. 2000).

3.2. *1997 June Outburst Spectra*

The upper panel of Figure 5 shows the spectra taken during the 1997 June outburst. All lines seen have been attributed to He I, though exact line identifications for the $\lambda = 2.16$–2.18 μm region are difficult to make. There is likely some contamination from the 2.1891 μm He II feature normally seen during quiescence. Doppler tomograms derived from the outburst spectra in Figure 5 are shown in Figure 6. Reduced χ^2 values of each fit are provided in Table 1. Finally, computed spectra, derived from the tomograms shown in Figure 6, are given in the lower panel of Figure 5.

The line profile behavior of the four He I lines appears at least marginally similar to that seen during quiescence: strong blueshifted emission at X-ray minimum and strong redshifted emission at X-ray maximum. However, the 2.0587 μm He I line in the outburst spectrum shows much stronger redshifted emission at $\Phi = 0.5$ than blueshifted emission at $\Phi = 0.0$ (Fig. 5; see also Fig. 4 of FHP99). Furthermore, in the region of the 2.0587 μm He I line, a narrow, permanently blueshifted absorption feature is seen, threaded through the background emission (Fig. 7).

The 2.1623 μm He I line appears almost double-peaked, though like the 2.0587 μm transition the peak velocities are a bit asymmetric, showing strongest emission while at maximum redshift. Double-peaked emission may be evidence for rotating gas in either an accretion disk or a wind. However, the stronger red peak also suggests these transitions may be contaminated by a P Cygni profile.

All three tomograms describe a ring structure similar to the tomographic signatures of an accretion disk (Fig. 6), consistent with rotational velocities on the order of 1000 km s^{-1}. Unfortunately, the mapping algorithm assumes that all line components have a velocity modulating symmetrically about γ. P Cygni profiles break this assumption, and it is possible that the entire ring structure in each map is the result of P Cygni absorption. P Cygni components will not be recreated in the computed spectra, and this explains the large discrepancies between the real data and fits in Figure 5. It is important that we consider only the real data in the upper panels when interpreting line behavior in this system. Note, though, that the fits are poor for the 2.0587 μm transition (Table 1) but improve for the other maps, suggesting that any P Cygni contributions are reduced in these transitions. Consequently, the case for a disk or rotating wind cannot be proven or ruled out in any of these transitions.

Fortunately, the sinusoidal absorption feature found in the 2.0587 μm spectral region is far less ambiguous, being clearly discerned over the entire temporal sequence of Figures 5 and 7. This continuous blue absorption feature was fit with a Gaussian to determine its velocity modulation over the orbital cycle. Without knowing the shape of the underlying emission profile, the fits to the absorption feature are dubious. However, since the absorption feature is narrow, being just a few resolution elements across, any bias to the result should be small. The feature was found to oscillate with a semiamplitude of $K = 109 \pm 13$ km s^{-1}. Most importantly, the phases of the velocity shifts, shown in Figure 8, are not like those seen in the N V and He II features during quiescence (Fig. 2) or like the He I emission features during outburst, whose red and blue maxima occur at $\Phi = 0.5$ and 0.0 (Fig. 4). Instead, the absorption shows red and blue maxima at phases $\Phi = 0.18$ and 0.68 (with an error of ~ 0.02), relative to the orbital ephemeris of Kitamoto et al. (1995).

If $\Phi = 0$ corresponds to superior conjunction of the compact object in Cyg X-3, red and blue maxima of features associated with the mass-donor He star should occur at

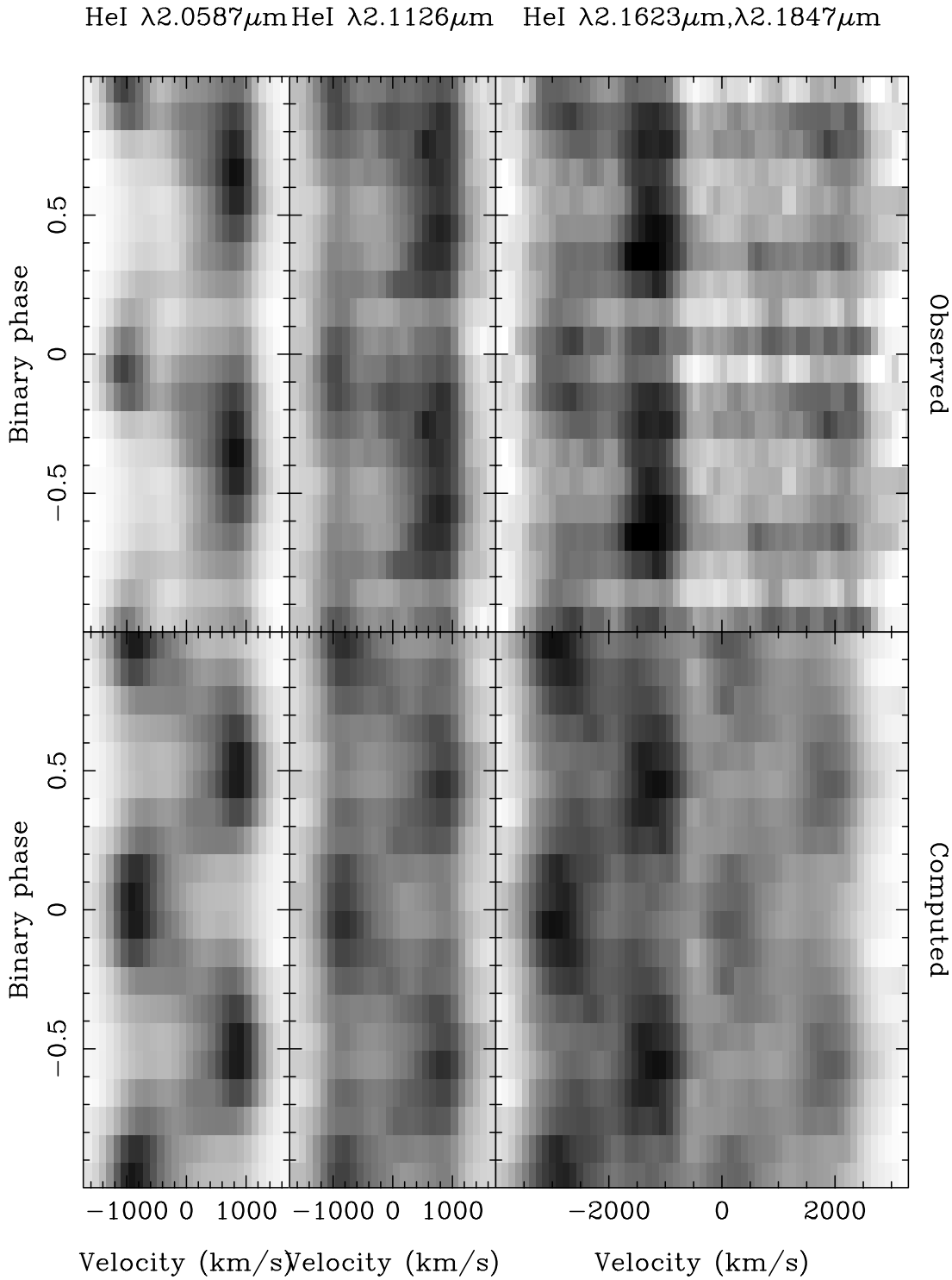

FIG. 5.—*K*-band trailed spectrograms representing full orbital phase coverage (4.8 hr) obtained on 1997 June 19. Spectral regions sampling the four strongest emission features of He I are displayed. The data have been repeated over a second orbital cycle. These data were obtained while Cyg X-3 was in outburst, as deemed by high radio and X-ray activity (see FHP99). The bottom panel shows the projected fits to the Doppler tomograms given in Fig. 6. Similar to Figs. 2 and 3, white to black corresponds to increasing emission intensity on individual linear scales, making white coincident with the continuum level.

$\Phi = 0.25$ and $\Phi = 0.75$, respectively. Thus the observed phasing of the absorption feature is approximately consistent with its tracing the motion of the He star. The impact of this result is explored further in § 4.1. Fixing the phases of the maximum blueshift and redshift to correspond with the binary phases $\Phi = 0.25$ and $\Phi = 0.75$ and refitting the radial velocity curves produce a fit only slightly poorer, $K = 100 \pm 14$ km s^{-1}, but with a consistent semiamplitude.

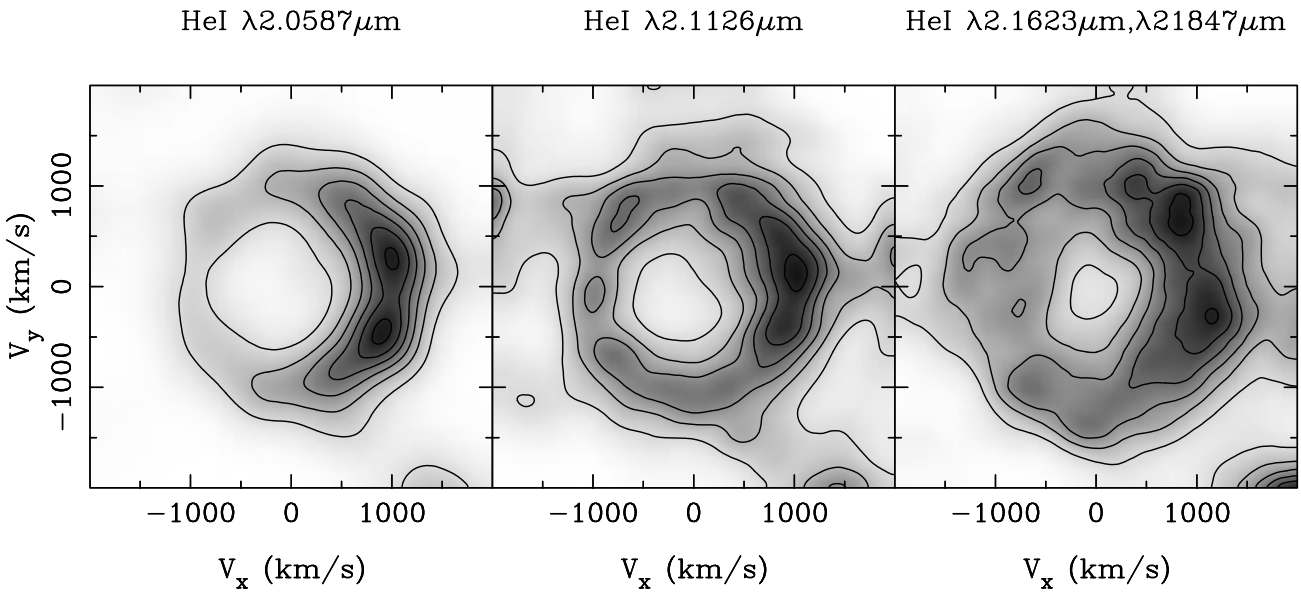

FIG. 6.—Doppler tomograms of the four He I lines during the 1997 June outburst, derived from the spectra given in the lower panel of Fig. 5. The intensity scales are as in Fig. 5.

4. DISCUSSION

4.1. *The* He I 2.0587 μm *Transition*

Some very important differences in the formation of the He I transitions have been described. This has lead to very different line fluxes and quite possibly different line profiles seen in the numerous lines detected in the Cyg X-3 outburst spectrum. First, 2.0587 μm emission is produced by direct radiative recombination into the 2 ^1P state or through recombinations at higher levels which then cascade down into the 2 ^1P state. This is not a problem in very dense extended winds, as the radiation field pumps electrons via the He I resonance lines into upper levels, leading to an enhancement of recombinations to the 2 ^1P level. However, once in this state, the atom has only a ~ 1 in 1000 chance of decaying via the 2.0587 μm (2 ^1P–2 ^1S) transition compared to the 584 Å (2 P^1–1 S^1) resonant transition. Thus strong 2.0587 μm emission further requires a very high optical depth in the 584 Å line. There is a second, equally important point about the He I 2.0587 μm line. Its lower level, 2 ^1S, is metastable and becomes increasingly overpopulated (relative to LTE). Frequently, a 2.0587 μm P Cygni profile is seen in hot, dense W-R winds because in the outermost regions the absorption process becomes quickly favored due to the overpopulated lower level (Williams & Eenens 1989). Thus, the expected behavior of the 2.0587 μm line in an extended wind is for it to self-absorb readily, i.e., create a P Cygni feature. It is of interest to note that several months after the outburst in 1997 June, the dominant feature in the spectrum of Cyg X-3 is the P Cygni profile occurring at 2.0587 μm (Fig. 1; see also FHP99).

The remaining transitions, most specifically the 4*s*–3*p* triplet at 2.1126 μm (the singlet 4*s*–3*p* line at 2.1138 μm has $\sim\frac{1}{3}$ the flux of the combined emission from the triplet transition), are not directly coupled to a resonance transition. Their emission level is set only by the recombination rate of He^+. Furthermore, they are not predisposed to increased absorption in dense winds like the 2.0587 μm transition, since their lower states readily cascade to lower levels. These differences can give rise to rather different behaviors in the He I lines seen in our outburst spectra and may possibly explain why the weak sinusoidal absorption feature seen threaded through the outburst spectrum shown in Figure 5 is detected only in the 2.0587 μm He I line.

4.2. *Orbital Dynamics from the* He I 2.0587 μm *Absorption Line*

Fortunately, an exact identification of the absorption feature seen in Figure 5 is not necessary for our purposes. While we feel confident that the feature is due to He I 2.0587 μm given the arguments above, even if the line is unknown or due to an unresolved blend of features, we can still use its velocity signature given in K to measure the orbital dynamics of the Cyg X-3 system. As already noted, the phasing of the absorption feature seems consistent with a source which is distributed approximately isotropically around the star and hence should reflect the binary motion of the He star in the system. However, before continuing with that interpretation, we note that there have been alternative suggestions for the phasing of the system. For example, Schmutz et al. (1996) propose that the He II and N V emission lines commonly observed in quiescence (Fig. 2) track the motion of the He star (in which case X-ray minimum light would be occurring a quarter of a cycle before superior conjunction of the compact accretor). So it is clear that there is not a consensus about the interpretation of the phasing in the Cyg X-3 system. As a result, we have investigated the implications of an origin for the absorption line in material centered on the accretor and on the donor.

Dynamical solutions for the first case, that the absorption line in the material is centered on the accretor, are presented in Figure 9*a*. The solid curves show the mass solution assuming the compact object is a neutron star of $M_X = 1.4$ $M_\odot$. For this solution only, two solid curves are given to demonstrate the error range on the velocity measurement (109 ± 13 km s^{-1}). This orientation, where the absorption

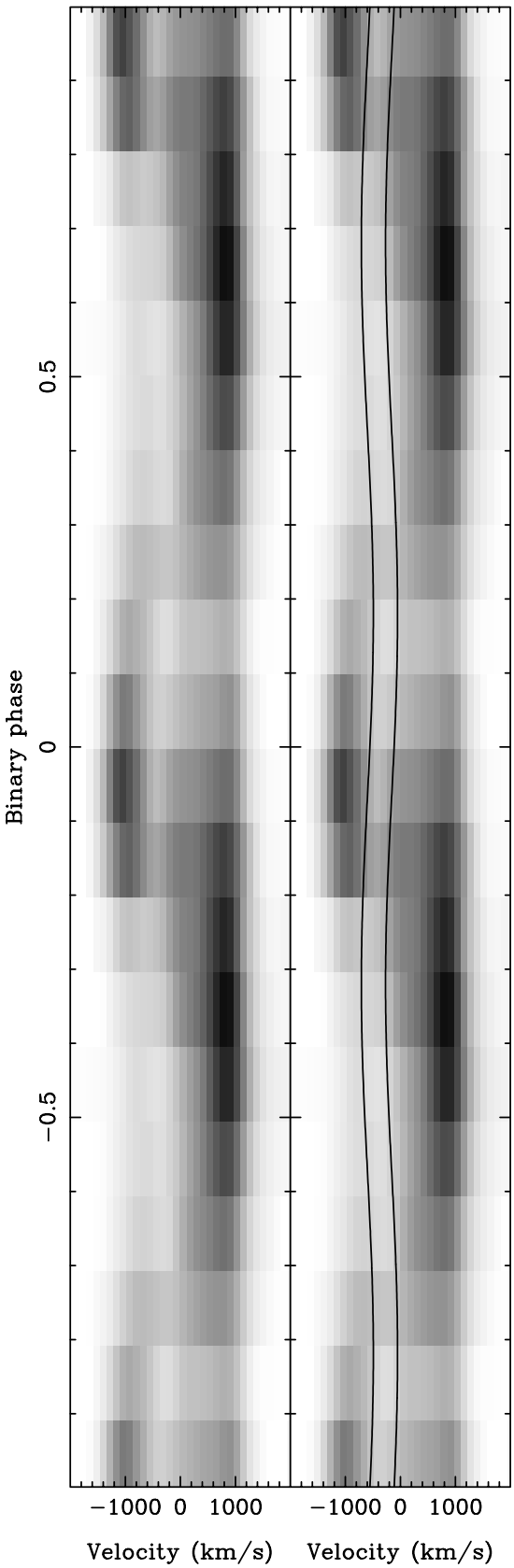

FIG. 7.—An expanded view of the full orbital phase coverage over a 4000 km s^{-1} velocity range centered on the He I 2.0587 μm line, as previously shown in Fig. 5. To the right is the same information, though marked with the location of the permanently blueshifted absorption feature. The absorption feature is seen as white against the broader, underlying emission feature of the 2.0587 μm He I line.

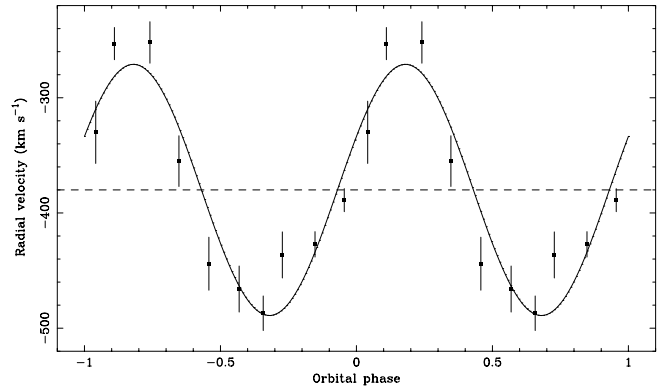

FIG. 8.—Gaussian fit to the absorption trough seen in the trailed, 2.0587 μm He I feature in Fig. 7, as a function of X-ray phase. Parameters of the fit include $K = 109 \pm 13$ km s^{-1}, with central velocity occurring at X-ray phase, $\Phi = -0.07 \pm 0.02$. If Φ is set equal to 0.0, the corresponding value for K, 100 ± 14 km s^{-1}, is nearly equally as good a solution. The values for K and Φ are independent of the exact identification of the spectral feature or features. The value for γ, shown in the above solution to be -380 ± 10 km s^{-1}, assumes the feature is due to the He I 2.0587 μm line. *See the electronic edition of the Journal for a color version of this figure.*

is centered on the accretor, is illustrated in Figure 9*b*. We see from Figure 9*a* that for all accretor masses, unless the He star is much less massive than implied from luminosity arguments (i.e., $\leq 2\ M_\odot$), the inclination of the system must be much lower ($\leq 50°$) than is generally accepted based on the X-ray and infrared modulations. Furthermore, any solution that allows for a reasonable inclination, $\geq 50°$, simultaneously gives an absurdly small, nearly nonphysical, value for the Roche lobe radius of the donor. As a result, we do not consider an origin for the absorption line in the accretion disk or any other material centered on the accretor to be very likely.

Rather, our analysis implies that the most likely configuration is the second case, that the material creating the absorption feature is centered on the mass donor. Solutions for this interpretation are presented in Figure 10*a*, and a schematic illustrating the orientation with phase is shown in Figure 10*b*. Again, two solid curves are given to illustrate the range of solutions consistent with the mass accretor being a neutron star, $M_X = 1.4\ M_\odot$, given our error on the velocity measurement. In this orientation, X-ray minimum occurs at superior conjunction of the accretor. It is immediately apparent from Figure 10*a* that realistic, high-inclination solutions are now available. Using this interpretation, we directly derive the mass function of the system, which is 0.027 $M_\odot$. The reason that this does not constrain at all the nature of the accretor is the large, probably dominant mass of the He donor star. For a neutron star accretor of 1.4 $M_\odot$, the mass of the He star is most likely in the range $5\ M_\odot \lesssim M_{WR} \lesssim 11\ M_\odot$, assuming that the system has a moderately high inclination, $i > 60°$.

However, if the accretor is a black hole, there is much less confidence about the mass of the He star. Charles (1998) lists derived masses for black holes in *low-mass* X-ray binaries and finds them to be in the range 5–12 $M_\odot$. Careful inspection of Figure 10*a* reveals that this allows a wide range of possible solutions, most of which are compatible with very large masses indeed (i.e., several tens of $M_\odot$) for the He star. This is because the Roche radius given in Figure 10*a* increases for greater He star mass and easily stays within the expected radius limit for such stars (Langer

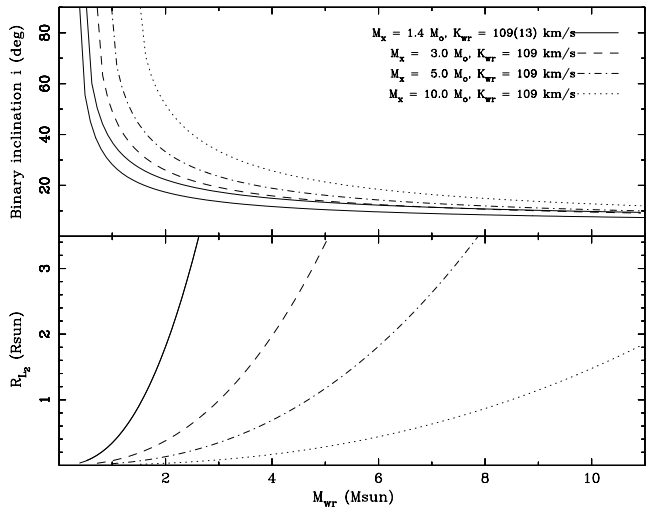

FIG. 9*a*

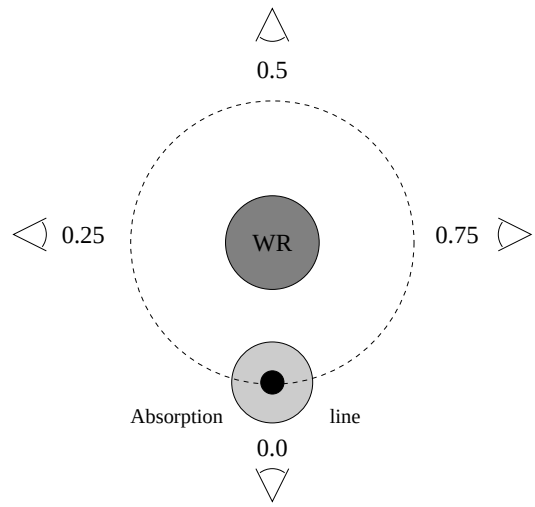

FIG. 9*b*

FIG. 9.—Orbital solutions assuming the motion traced in Figs. 7 and 8 is centered on or associated with the motion of the compact object. Panel *a* shows orbital solutions for differing input masses of the companion (W-R) object, displayed vs. inclination angle of the binary system and Roche lobe radius. Solutions explored range from a compact object mass $M_X = 1.4$ to 10 $M_\odot$. Two solid curves are given for the $M_X = 1.4\ M_\odot$ solution, which illustrates the plus-minus error range on K. For any reasonable W-R star mass, $M > 2\ M_\odot$, only extremely low inclinations are possible. This is difficult to reconcile with the X-ray modulation. The orbital orientation implied by this interpretation is indicated in panel *b*. Such an interpretation is counterintuitive in the sense that it requires X-ray orbital minimum to occur when the X-ray source is nearest to the observer. All of these evidences disfavor the interpretation that the sinusoidal variations are centered on or associated with motion of the compact object. *See the electronic edition of the Journal for a color version of this figure.*

1989). Moreover, the Roche radius of the He star shown in Figure 10*a* can even be less than its R_*, as shown in Langer's Figure 5. This is because the tenuous outer atmospheric radius of the star, identified as R_*, contributes an insignificant fraction of the mass of the star and can extend well beyond the dynamical Roche radius. Nonetheless, we see from Figure 10*a* that solutions for an $M_{BH} \gtrsim 10\ M_\odot$ would be inconsistent with our assumption of even a moderate inclination for the binary system, for any realistic companion star mass $M_{WR} \lesssim 70\ M_\odot$. For this reason, we put an upper limit on the mass of the compact object of $M_{BH} \lesssim 10\ M_\odot$. The well-known high-mass X-ray binary system Cyg X-1 has a similar mass estimate for its black hole (Charles 1998).

We note that in the binary orientation proposed by Schmutz et al. (1996), which lead them to argue for a most likely value of $M_{BH} \approx 17\ M_\odot$ for the compact object, the absorption feature would be required to arise from a region centered not on the He star or accretor, but a quarter of a cycle out of phase with either orientation.

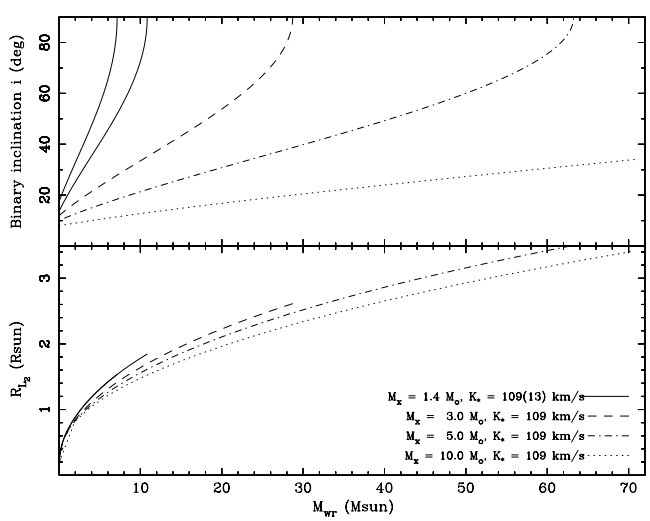

FIG. 10*a*

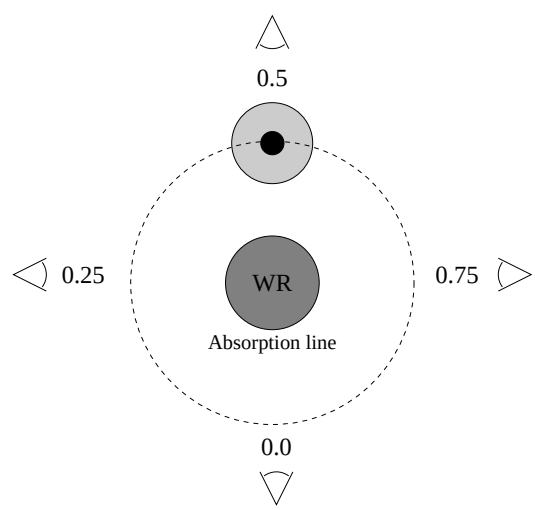

FIG. 10*b*

FIG. 10.—Orbital solutions assuming the motion traced in Figs. 7 and 8 is centered on or associated with the motion of the mass-donor He star. Panel *a* shows orbital solutions for differing input masses of the compact object, $M_X = 1.4$ to 10 $M_\odot$, displayed vs. inclination and Roche lobe radius. Two solid curves are given for the $M_X = 1.4\ M_\odot$ solution, which illustrates the plus-minus error range on K. This second set of solutions allows for the high inclination suggested by the X-ray and infrared modulation simultaneously with moderately high mass solutions and Roche lobe radii for the mass donor. The orbital orientation implied by this interpretation is indicated in panel *b*. It allows for X-ray orbital minimum to occur when the X-ray source is farthest from the observer, at superior conjunction. This configuration gives the most reasonable set of solutions for the orbit of the Cyg X-3 system. *See the electronic edition of the Journal for a color version of this figure.*

4.3. *The Nature of the Stellar Companion*

The assumptions used to determine stellar mass in Figure 10*a* also provide limits for the radius of the stellar companion of Cyg X-3. We are able to test whether this result is consistent with the characteristics, most specifically the luminosity, predicted from atmosphere models and observations of typical W-R stars.

The distance to Cyg X-3 is not directly known. However, Dickey (1983) has suggested a lower limit on the distance, $11.6 \times \pi/10$ kpc, where π is the distance in kiloparsecs to the Galactic center, based on the detection of high-velocity neutral hydrogen absorption features and applying a flat rotation curve for the Galaxy. With an updated value for the distance to the Galactic center of ~ 8 kpc (Reid 1993), this gives a lower limit to Cyg X-3 of ~ 9 kpc. Original estimates of the line-of-sight extinction to Cyg X-3, $A_V = 15$, were made by Becklin et al. (1973). More recent measurements suggest a slightly higher value of $A_V = 19$ (Molnar et al. 1988), $A_J = 5.5$ (van Kerkwijk et al. 1996), which corresponds approximately to $A_V = 19$ and $A_J = 6.0$ (Fender et al. 1996), corresponding approximately to $A_V = 20.5$ (Rieke & Lebofsky 1985). Determining the line-of-sight extinction is dependent on measuring the flux distribution over a large enough wavelength range to note the differential change, as done by both van Kerkwijk et al. (1996) and Fender et al. (1996). But equally importantly, one must simultaneously make assumptions about the functional form of that extinction and the functional form of the underlying continuum of the source. For this reason, without an *a priori* quantitative understanding of the stellar companion, the line-of-sight extinction cannot be as well constrained as one might hope. Mindful of these limitations, we have used the apparent magnitudes of Cyg X-3 given by Wagner et al. (1989) and Fender et al. (1996), $m_I = 20.0$, $m_H = 13.11$, and $m_K = 11.76$, and applied an extinction of approximately $A_V = 20$ and a distance of 9 kpc to obtain absolute magnitudes of $M_I = -4.8$, $M_H = -5.2$, and $M_K = -5.1$ for the stellar companion. It is precisely these values, the very luminous lower limits for the absolute magnitude of the stellar companion, that most strongly challenge the notion of Cyg X-3 being a low-mass X-ray binary system (Mitra 1998).

We have argued that, while in quiescence, the emission lines seen in Cyg X-3, presumably dominated by the companion star, look most similar to the lines seen in early WN-type (WNE) W-R stars (FHP99). Based on direct measurements of WNE stars given in Smith, Meynet, & Mermilliod (1994), a mass range from 6 to 12 $M_\odot$ corresponds to a typical absolute magnitude $-4 > M_V > -4.8$. Naturally, there is a large scatter in the observed relation. Without a direct determination of M_V, with the uncertainties in the bolometric correction, and with the difficulty in extrapolating the extinction characteristics toward Cyg X-3, the luminosity for the stellar component of Cyg X-3 is not highly inconsistent with the luminosity of other WNE stars.

4.4. *The Nature of the Accretor*

The crucial question of whether the accretor is a neutron star or a black hole cannot be decided with confidence. The only *direct* observational evidence for the presence of a neutron star in Cyg X-3 was in the report of 12.6 ms γ-ray pulsations, about 15 years ago (Chadwick et al. 1985). However, this result has never been widely accepted. As already stated, Schmutz et al. (1996) argued that the observational evidence supports a black hole accretor, which prompted Ergma & Yungelson (1998) to investigate the evolution of such a system. They concluded that Cyg X-3 *may* contain a black hole accreting at super-Eddington rates. Mitra (1998), however, argued strongly *against* the interpretation of Schmutz et al. (1996), preferring a low-mass system (which is extremely hard to reconcile with the very high luminosity of the system). For now we will have to consider a fairly large range of accretor masses up to $M_{\rm BH} \lesssim 10\ M_\odot$ (see discussion in § 4.2).

5. CONCLUSIONS

The X-ray binary Cyg X-3 is the only known system containing a (presumably) massive He star with a compact object. This makes Cyg X-3 a uniquely important link in our understanding and testing of massive X-ray binary evolution. In this paper we pursued an emission-line analysis of the quiescent and outburst spectra presented in FHP99. We reported that while the double-peaked emission seen in the He I lines during outburst are consistent with a disk-wind geometry as proposed in FHP99, our tomographic analysis in particular reveals unresolvable ambiguities in the mechanism responsible for the formation of double-peaked emission. For this reason, additional constraining spectral information or methods are needed to resolve the nature of the double-peaked emission and its relation to the wind or disk geometry of the system during outburst.

Of greater significance was the detection of a weak absorption feature threading through the blue wing of the 2.0587 μm He I line. This feature moves $\sim \frac{1}{4}$ of an orbit out of phase with all other spectral modulations seen in Cyg X-3, consistent with He I absorption originating in an isotropic, asymptotic wind from the companion star. Consequently it can be used to derive the first radial velocity curve for the Cyg X-3 system. Employing reasonable geometric assumptions, we derive a mass range of $5\ M_\odot \lesssim M_{\rm WR} \lesssim 11\ M_\odot$ for the He star, if the accretor is a neutron star. Additionally, should the accretor be a black hole, we determine $M_{\rm BH} \lesssim 10\ M_\odot$, based on an upper mass limit, $M \lesssim 70\ M_\odot$, for the He star companion.

Identification of the critical absorption feature used in obtaining a mass function for the Cyg X-3 system was made possible only through phase-resolved near-infrared observations. A further key was obtaining observations during outburst. Clearly, periods of high X-ray variability would make the most opportune times to catch this rare infrared state once more. The spectra presented in FHP99 represent the best quality spectra a 4 m class telescope will likely ever deliver on this object, and yet these spectra barely detect the very weak, sometimes very broad, and often heavily blended features. Its not certain that moving to an 8 m class telescope would resolve all the problems with the current data set, as many of the lines are already resolved with the current spectra. However, the narrow absorption feature detected in the outburst spectrum may be just the first of many similarly weak and narrow features which might better be revealed with higher quality spectra. Such features offer promise in resolving the ambiguities plaguing our analysis.

FHP99 showed there to be a marked decrease in X-ray flux during the 4 days prior to the near-infrared outburst,

the minimum occurring just after outburst. This may have resulted from drops in the ionization state of the wind following a temporary decrease in the X-ray flux. FHP99 showed that the outburst occurring in 1997 June and previous outbursts suggested in earlier spectra (van Kerkwijk et al. 1996) were short lived (≤ 24 hr). Careful day-to-day monitoring of Cyg X-3 in the X-ray and radio, particularly during epochs of high X-ray and radio activity, would potentially precede suitable windows for near-infrared spectroscopic observations of P Cygni lines.

We are grateful for comments made by our referee which lead us to greatly improve the presentation of this work. Observations reported in this paper were obtained with the Multiple Mirror Telescope, operated by the Smithsonian Astrophysical Observatory and the University of Arizona. We are grateful to G. and M. Rieke for their critical support in this program. M. M. H. received support for this work provided by the University of Cincinnati through a University Research Council Grant and a Faculty Summer Fellowship.

REFERENCES

Becklin, E. E., Neugebauer, G., Hawkins, F. J., Mason, K. O., Sanford, P. W., Mathews, K., & Wynn-Williams, C. G. 1973, Nature, 245, 302
Burrows, A., & Woosley, S. E. 1986, ApJ, 308, 680
Chadwick, P. M., Dipper, N. A., Dowthwaite, J. C., Gibson, A. I., & Harrison, A. B. 1985, Nature, 318, 642
Charles, P. A. 1998, in Theory of Black Hole Accretion Discs, ed. M. A. Abramowicz, G. Björnsson, & J. E. Pringle (Cambridge Contemporary Astrophys.; Cambridge: Cambridge Univ. Press), 1
Conti, P. 1996, in Wolf-Rayet Stars in the Framework of Stellar Evolution, ed. J. M. Vreux, A. Detal, D. Fraipont-Caro, E. Gosset, & G. Rauw (Liege: Univ. Liege, Inst. d'Astrophys.), 655
Dickey, J. M. 1983, ApJ, 273, L71
Ergma, E., & Yungelson, L. R. 1998, A&A, 333, 151
Fender, R. P., Bell Burnell, S. J., Williams, P. M., & Webster, A. S. 1996, MNRAS, 283, 798
Fender, R. P., Hanson, M. M., & Pooley, G. G. 1999, MNRAS, 308, 473 (FHP99)
Hulse, R. A., & Taylor, J. H. 1975, ApJ, 195, L51
Kitamoto, S., et al. 1995, PASJ, 47, 233
Langer, N. 1989, A&A, 210, 93
Lépine, S., & Moffet, A. F. J. 1999, ApJ, 514, 909
Marsh, T. R., & Horne, K. 1988, MNRAS, 235, 269
Mason, K. O., Cordova, F. A., & White, N. E. 1986, ApJ, 309, 700
Mitra, A. 1996, MNRAS, 280, 953
Mitra, A. 1998, ApJ, 499, 385
Molnar, L. A., Reid, M. J., Grindlay, J. E., & Willner, S. P. 1988, BAAS, 20, 736
Morris, P. W., Eenens, P. R. J., Hanson, M. M., Conti, P. S., & Blum, R. D. 1996, ApJ, 470, 597
Paerels, F., Cottam, J., Sako, M., Liedahl, D. A., Brinkman, A. C., van der Meer, R. L. J., Kaastra, J. S., & Predehl, P. 2000, ApJ, 533, L135
Parsignault, D. R., et al. 1972, Nature Phys. Sci., 239, 123
Reid, M. J. 1993, ARA&A, 31, 345
Rieke, G. H., & Lebofsky, M. J. 1985, ApJ, 288, 618
Sanford, P. W., & Hawkins, F. H. 1972, Nature Phys. Sci., 239, 135
Schalinski, C. J., et al. 1998, A&A, 329, 504
Schmutz, W., Geballe, T. R., & Schild, H. 1996, A&A, 311, L25
Skilling, J., & Bryan, R. K. 1984, MNRAS, 211, 111
Smith, L. F. 1968, MNRAS, 138, 109
Smith, L. F., Meynet, G., & Mermilliod, J.-C. 1994, A&A, 287, 835
van den Heuvel, E. P. J., & De Loore, C. 1973, A&A, 25, 387
van Kerkwijk, M. H., et al. 1992, Nature, 355, 703
van Kerkwijk, M. H., Geballe, T. R., King, D. L., van der Klis, M., & van Paradijs, J. 1996, A&A, 314, 521
Wagner, R. M., Kreidl, T. J., Bus, S. J., & Williams, W. 1989, ApJ, 346, 971
Williams, D., Thompson, C. L., Rieke, G. H., & Montgomery, E. 1993, Proc. SPIE, 1946, 482
Williams, P. M., & Eenens, P. 1989, MNRAS, 240, 445